Journal of Renewable and Sustainable Energy

RESEARCH ARTICLE | SEPTEMBER 04 2024

Power output fluctuations and unsteady aerodynamic loads of a scaled wind turbine subjected to periodically oscillating wind environments

Emmanuvel Joseph Aju ; Pengyao Gong ; Devesh Kumar ; Mario A. Rotea ; Yaqing Jin ✉

J. Renewable Sustainable Energy 16, 053301 (2024)
https://doi.org/10.1063/5.0219853

Journal of Renewable and Sustainable Energy
ARTICLE
pubs.aip.org/aip/rse

Power output fluctuations and unsteady aerodynamic loads of a scaled wind turbine subjected to periodically oscillating wind environments

Cite as: J. Renewable Sustainable Energy **16**, 053301 (2024); doi: 10.1063/5.0219853
Submitted: 20 May 2024 · Accepted: 18 August 2024 ·
Published Online: 4 September 2024

Emmanuvel Joseph Aju,[1] Pengyao Gong,[1] Devesh Kumar,[2] Mario A. Rotea,[1] and Yaqing Jin[1,a)]

AFFILIATIONS

[1]Center for Wind Energy and Department of Mechanical Engineering, The University of Texas at Dallas, Richardson, Texas 75080, USA
[2]Center for Wind Energy and Department of Electrical and Computer Engineering, The University of Texas at Dallas, Richardson, Texas 75080, USA

[a)]Author to whom correspondence should be addressed: yaqing.jin@utdallas.edu

ABSTRACT

Wind tunnel experiments were performed to quantify the coupling mechanisms between incoming wind flows, power output fluctuations, and unsteady tower aerodynamic loads of a model wind turbine under periodically oscillating wind environments across various yaw misalignment angles. A high-resolution load cell and a data logger at high temporal resolution were applied to quantify the aerodynamic loads and power output, and time-resolved particle image velocimetry system was used to characterize incoming and wake flow statistics. Results showed that due to the inertia of the turbine rotor, the time series of power output exhibits a distinctive phase lag compared to the incoming periodically oscillating wind flow, whereas the phase lag between unsteady aerodynamic loads and incoming winds was negligible. Reduced-order models based on the coupling between turbine properties and incoming periodic flow characteristics were derived to predict the fluctuation intensity of turbine power output and the associated phase lag, which exhibited reasonable agreement with experiments. Flow statistics demonstrated that under periodically oscillating wind environments, the growth of yaw misalignment could effectively mitigate the overall flow fluctuation in the wake region and significantly enhance the stream-wise wake velocity cross correlation intensities downstream of the turbine hub location.

I. INTRODUCTION

In the past decade, the utilization of wind energy has increased more than six times, making it one of the most accessible and rapidly advancing renewable energy sources in the United States.[1] Abrupt fluctuations in wind speed can significantly amplify power output variations and the fatigue loading experienced by wind turbines.[2–4] Extreme loads in gust events can also lead to significant and occasionally catastrophic damage to the turbine, such as tower strike,[5] in addition to fatigue failure from dynamic loads.

The formation of eddies in the atmospheric boundary layer is influenced by the local pressure gradients and near-ground friction. Interaction between eddies varying in size and strength may result in sudden acceleration or deceleration of wind velocities, or "gusts." Additionally, certain climatic factors such as frontal activity, steep pressure gradients, or convective weather are linked to the creation of gusts.[6] Typically, major temporal and spatial events such as cyclones produce the most violent wind gusts.[7,8] One aspect that unites the many different definitions of wind gusts found in the literature is the mention of "spontaneous" variations in wind speed.[9] According to Branlard,[10] gust is a wind speed variation within a short period of time. The author also conveyed that acceleration of wind speed, positive gust, and deceleration of wind speed, negative gust, both can cause a sharp increase in loads on turbines. Similar to this, a gust is defined as a brief change in wind speed that can be distinguished by its rising time, magnitude, and duration in the IEC 61400-1 turbine safety standard.[11] It is worth noting that in addition to gust winds formed by atmospheric dynamics, the operation conditions of wind turbines may also produce equivalent periodically oscillating inflows impinging on their rotors. For instance, floating offshore wind turbines encounter periodically oscillating inflow episodes when observed from the turbine's frame of reference due to their pitching motions.[12–16] In addition, onshore horizontal axis wind turbines under dynamic yawing could have comparable aerodynamic loads to a stationary wind turbine when subjected to periodically oscillating inflow. Such wind gusts impact power output stability and can result in structural damage to turbine components.[17,18] The identification, description, and assessment of the interaction mechanisms between unsteady incoming winds, turbine power output fluctuations, and aerodynamic loads during periodically oscillating inflows have the potential to reduce expenses associated with operations and maintenance, mitigate system risks through ongoing monitoring, establish early warning systems for potential malfunctions, and facilitate the creation of control systems to mitigate unwanted dynamics[19] due to the aforementioned interactions.

Most studies on the interactions between turbine performance and unsteady incoming flows have primarily concentrated on scenarios where the turbine rotor is perpendicular to the wind direction. Recently, there has been a growing focus on turbines operating under yaw misalignment due to their potential to enhance the overall power output of an entire wind farm. Yaw misalignment between the flow direction and the upstream turbines can be accomplished with wake steering, which results in lower power output on these units but higher overall velocities for the downstream turbines. Early experimental studies on horizontal axis wind turbine wake and visualization of wake deflection due to yaw misalignment were conducted by Grant *et al.*[20] and Grant and Parking.[21] They demonstrated that the wake skew angle for the three-blade turbine is greater than that for the two-blade equivalent by examining the wake deflection of turbines with two and three blades under yaw misalignment. In the past 5 years, a number of theoretical, computational, and experimental investigations have been carried out to analyze the impact of yaw misalignment on wake development and turbine performance. These studies have drawn the following conclusions: (i) The influence of the counter-rotating vortex pair (CVP) causes the wake stream-wise velocity deficit to have a kidney-shaped cross section.[22–27] (ii) Depending on how the ground interacts with the CVP, the yawed turbine wakes will migrate in either a vertically upward or downward direction.[22,27] (iii) The wake flow is gradually redirected as the yaw angle increases, creating an asymmetric velocity deficit with respect to the rotor centerline.[22] (iv) Yaw misalignment affects both power coefficient (C_p)[28,29] and thrust coefficient (C_T).[28,30] The aforementioned phenomena were proven recently by Bartl *et al.*[31] by an experimental investigation of the impact of incoming turbulence and shear on the wake of a yawed turbine. Analytical models that are straightforward and computationally affordable can be used to assess how well yaw control affects wake velocity distributions. Shapiro *et al.*[26] modeled the wake of a yawed turbine by utilizing a lifting surface assumption for the rotor. Bastankhah and Porté-Agel[22] created a realistic analytical model to forecast both span-wise and stream-wise wake velocities utilizing the decomposition of Reynolds-averaged Navier–Stokes equations with experimental data.

Despite the progress made to understand the impact of periodically oscillating wind environments on the performance and fatigue loading of wind turbines, the underlying physics of the coupling mechanisms between time-varying incoming wind speed, instantaneous turbine power output, and unsteady aerodynamic loads remains obscure. In particular, predictive models that allow to quantify wind turbine performance and unsteady loading under various periodically oscillating wind amplitudes, frequencies, and turbine yaw angles are currently lacking, which is a precursor to optimizing the turbine design across various flow environments and operation conditions. Motivated by this challenge, this study focuses on how wake flows, power output fluctuations, and unsteady aerodynamic loads on turbines under yaw misalignment in the presence of periodically oscillating inflow winds are fundamentally coupled. Systematic wind tunnel tests were carried out with a model turbine to quantify the unsteady power outputs, thrust loads on the turbine tower, and wake flow statistics with various yaw misalignment angles, incoming periodically oscillating wind magnitudes, and frequencies. Furthermore, a computationally efficient reduced-order physical model was built based on local incoming flow dynamics and turbine parameters to emphasize the dominant elements affecting the variations of turbine power output and aerodynamic loads. To the best of the authors' knowledge, this is the first study providing a comprehensive analysis of the power and wind load fluctuations for a turbine under yaw misalignment and periodically oscillating inflows with integrated experimental campaigns and modeling. *This work is important for filling the current knowledge gap of predicting* and *controlling the power output stability as well as turbine fatigue loading when applying wake steering in the presence of periodically oscillating winds*. The manuscript is organized as follows: Sec. II describes the experimental setup; Sec. III illustrates the results, discussion, and modeling; and conclusions are summarized in Sec. IV.

II. EXPERIMENTAL SETUP

Wind tunnel experiments were performed to investigate the influence of periodically oscillating winds on turbine power output, aerodynamic load, and wake statistics under yaw misalignment. A model wind turbine with a yaw mechanism was placed on the bottom wall of the Boundary Layer and Subsonic Tunnel (BLAST) at the University of Texas at Dallas. The boundary layer test section of BLAST is 2.1 m high, 2.8 m wide, and 30 m long. More details of the wind tunnel are provided in the study by Aju *et al.*[32]

The horizontal-axis wind turbine was designed based on the model from Bastankhah and Porté-Agel[33] and manufactured from the Stratasys F370 3D printer at the University of Texas at Dallas. The turbine has a rotor diameter of $d_T = 200\,\text{mm}$, and the hub height is $z_{hub} = 200\,\text{mm}$. The turbine tower was made from a M10 threaded rod. Details of the turbine blade geometry across various sections are provided in the study by Bastankhah and Porté-Agel[33] and are not duplicate here for brief. A DCX16L Maxon motor was used as the generator with a diameter of 16 mm, which was attached with a 1 ohm resistance as the load to control the rotating speed of the turbine. This led to a rotational speed of $\Omega \approx 1760 RPM$, which in turn produces a tip–speed ratio of $\lambda = \Omega R/U_0 \approx 4$, with a power coefficient of $C_p = 0.35$, and a thrust coefficient of $C_T = 0.8$ in the free-stream condition. The implementation of constant resistance led to the variation of turbine rotation speeds as a function of incoming wind velocities. For the DCX16L Maxon motor, the rotational speed of the generator is proportional to the generator voltage, where the generator torque, τ, is proportional to the current of the generator.[33] Hence, with a constant resistance, the torque of the generator is proportional to the rotational velocity of the generator, i.e., $\tau \propto \Omega$. Similar turbine properties were used in other experimental works with miniature wind turbines.[12,34] The yaw mechanism for the turbine was engineered utilizing Actobotics SG-12 series gearbox and operated through Arduino Mega

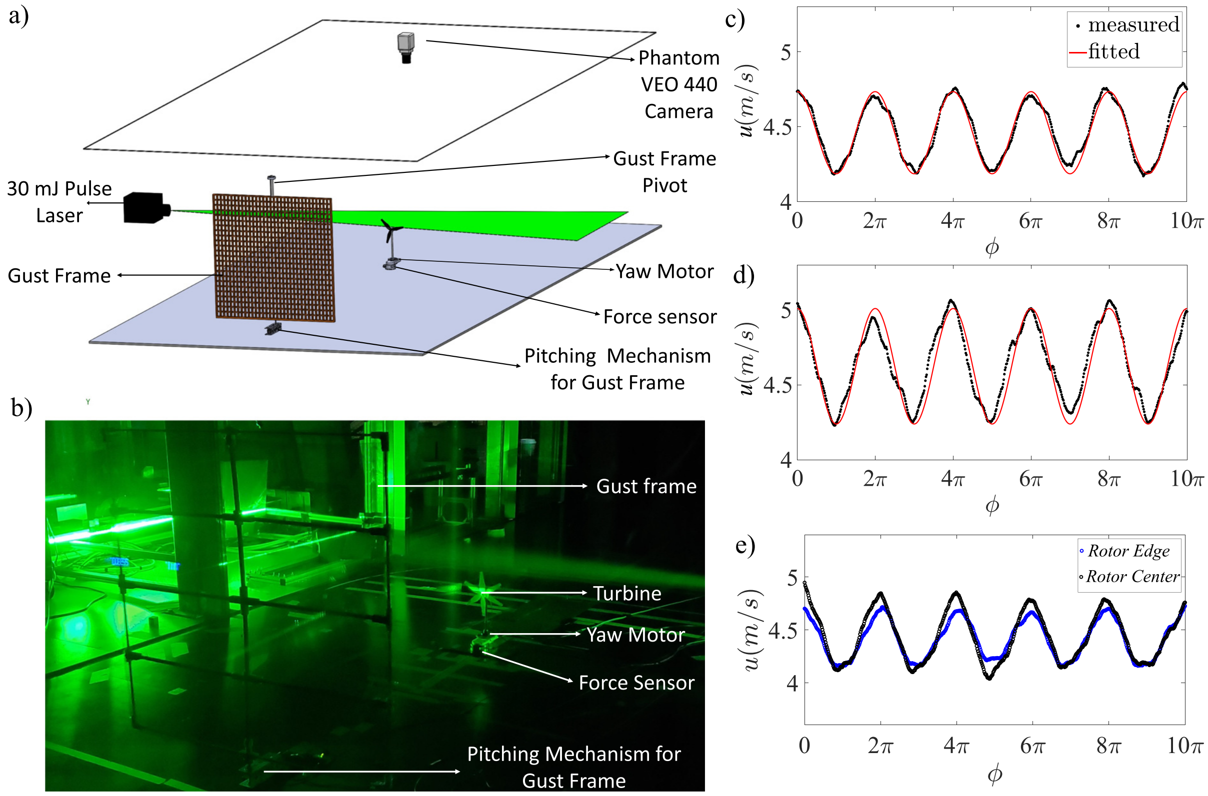

FIG. 1. (a) Schematic of the experimental setup. (b) Photograph of the particle image velocimetry (PIV) measurement inside the wind tunnel. (c) Selected time series of measured incoming fluctuating wind velocities as a function of phase angle, ϕ, and the corresponding sinusoidal fitting at frame yaw amplitude of $A = 60^\circ$ and frequency of $f = 1$ Hz; (d) is the same as (c) but at frame yaw amplitude of $A = 90^\circ$. (e) A representative time series of stream-wise velocity for frame yaw amplitude of $A = 60^\circ$ and frequency of $f = 1$ Hz at two span-wise locations, as a function of phase angle, ϕ.

and the Laboratory Virtual Instrument Engineering Workbench (LabVIEW). Additional information regarding the yaw control mechanism can be found in the publication by Kumar *et al.*[35] The periodically oscillating inflow was produced using a mesh affixed to a wooden frame with dimensions of $5d_T$ in width and $5d_T$ in height. It was placed inside BLAST $5d_T$ upstream of the turbine [Figs. 1(a) and 1(b)]. We used a 5202 series yellow jacket DC motor from Servo-City to yaw the frame about its midsection to generate periodically oscillating wind, and the frame yaw angles were controlled to behave as sinusoidal variations in the form of $\theta = A\sin(2\pi f t)$. In this work, three yaw frequencies $f = 0.6$, 0.8, and 1 Hz, and two frame yaw amplitudes $\mathrm{A} = 60^\circ$ and 60°, were investigated in the wind tunnel tests. This yaw frame system produced sinusoidal wind velocity fluctuations at the location of the model turbine, as shown in Figs. 1(c) and 1(d), where the local incoming wind can be fitted in the form of $u(t) = U_0 + U_A\sin(2\pi f t)$ and $U_0 = 4.6 \pm 0.1\ \mathrm{m\,s^{-1}}$ is the mean incoming flow velocity at the turbine hub. Figure 1(e) shows a representative periodic incoming flow at two different positions along the span: at the edge of the turbine rotor and at the center of the turbine rotor. In general, it is evident that the generated periodic incoming flow has relatively similar amplitude and phase in both span-wise locations, and similar phenomenon was observed under all incoming flow conditions. The periodic incoming wind frequencies are scaled using the corresponding non-dimensional flow fluctuation frequency, quantified as $k = \frac{2\pi f d_T}{U_0} = 0.16, 0.21$, and 0.27, whereas the flow fluctuation intensities $\frac{U_A}{U_0}$ are summarized in Table I. These periodically oscillating frequencies, when scaled up based on the ratio of rotational velocities, are on the order of 3-min time periods. This is comparable to the time periods observed in utility-scale turbines experiencing periodically oscillating inflow, such as those affected by wake meandering of an upstream turbine,[36] dynamic yaw control,[37] and floating offshore wind turbines.[38]

It is important to note that the turbine is not a scaled-down version of a reference turbine but is specifically designed for high efficiency

TABLE I. Consecutive flow fluctuation intensity U_A/U_0 as a function of frame yaw frequency and amplitudes.

Frame yaw amplitude A (°) \ Frame yaw frequency f (Hz)	0.6	0.8	1
60	0.16	0.14	0.11
90	0.24	0.21	0.18

at low Reynolds numbers in the wind tunnel. The scaling of model turbine to utility scale turbines can be done using scaling factors and non-dimensional numbers.[39] The length scaling factor can be defined as ratio of characteristic lengths, $n_l = d_T/D_T$, where D_T is the diameter of the utility scale turbine. The time scaling factor can be defined as $n_t = t_T/T_T$, where T_T is the characteristic time of the utility scale turbine, whereas frequency scaling factor is inverse of time scaling factor.

The instantaneous turbine power output was inferred by the voltage of the DC motor measured directly via a USB-6210 datalogger from National Instruments. For each experiment, the voltage was sampled at a frequency of 1 kHz with 50 incoming wind velocity fluctuation cycles. In addition, we investigated the unsteady aerodynamic loads on the tower, which is an essential part of the turbine with 30% of the turbine's net cost.[40] The measurements of wind loading were achieved by an ATI high-resolution six-axis load cell connected to the turbine tower. During each experiment, the measurement of instantaneous thrust loads (the force aligned with the incoming flow direction) was synchronized with the turbine power output measurement, and the uncertainty of the load cell was less than 1.2%. Complementary time-resolved particle image velocimetry (PIV) measurements were performed to characterize the turbine wake flow dynamics. A high-speed Phantom VEO440 camera with 4 MP resolution was used to create a field of view (FOV) of $442 \times 276\,\text{mm}^2$ to investigate the mean and unsteady wake flows. The FOV in the turbine wake region was parallel to the bottom wall and located within a stream-wise distance of $x/d_T \in [2.5, 4.7]$ and a side-wise distance of $y/d_T \in [-0.5, 0.5]$, where the coordinate system was defined with the origin coincident with the rotor center. The FOV was illuminated by a 1-mm-thick laser sheet generated from a 30 mJ/pulse laser, where airflow was seeded by 15-μm-diameter soap bubbles from the TSI bubble generator. The soap bubbles were well mixed by the recirculating wind tunnel before each experiment. For each experiment, 4000 image pairs were collected, which included 100 image pairs per cycle of periodically oscillating wind by changing the camera capturing frequency. These image pairs were then processed using the Insight4G software package from TSI with a multipass scheme. The final interrogation window size was 32×32 pixels with 50 % overlap, resulting in a final vector grid spacing $\Delta x = \Delta y = 2.4$ mm. The overall uncertainty of the identified seeding particle locations was ~0.1 pixel; this led to the uncertainty of flow velocity measurement of ~1.4% given the bulk particle displacement of 7 pixels between two successive images.

III. RESULT, DISCUSSION, AND MODELING

In this section, we discuss in detail the distinctive variation of turbine power output, aerodynamic loads, and wake statistics under various incoming periodically oscillating flow conditions and yaw misalignment angles. Special attention will be paid to turbine power output fluctuations and unsteady wind loads with both experimental measurements and modeling. The fluctuations of all the variables are calculated based on the mean values of the time series, without filtering out the inflow periodicity.

A. Unsteady power output

This section is dedicated to formulating a theoretical framework that utilizes measured incoming periodically oscillating flow as an input parameter in order to forecast the unsteady power and aerodynamic loads of the turbine during periodically oscillating wind episodes and under yaw misalignment. First, a representative time series of turbine power output $P(t)/P_0$ superimposed with instantaneous incoming wind velocities $u(t)$ is shown in Fig. 2. Here, P_0 is the mean power output of the turbine with no yaw misalignment (i.e., $\psi = 0°$). Due to the presence of periodically oscillating wind, $P(t)$ exhibited quasi-sinusoidal temporal variations regardless of turbine yaw angles ψ. The periodic measured data exhibits high-frequency oscillations due to the turbulence generated by the presence of gust frame. The incoming flow itself produced by the wind tunnel has negligible turbulence intensity of $I_u \approx 0.1\%$. It is worth noting that the time series of $P(t)$ demonstrated a distinct phase-delay $\Delta\phi$ with respect to $u(t)$ across all investigated conditions, where the local maximum of $P(t)$ during each cycle appeared when $u(t)$ decreased close to its mean value. This phase-shift delay is due to the wind turbine dynamics. Thus, to quantify this problem, we need to consider the effects of turbine rotor inertia. The dynamic inflow effect is not considered for the miniature turbine because the characteristic timescale for dynamic inflow effects given by Mancini *et al.*[41] as $\tau_1 \approx \frac{d_T}{U_0} \approx 0.04$ s is approximately two orders of magnitude smaller than the time scales of the periodically oscillating inflow considered in this study. Therefore, since the periodic inflow changes at a much slower rate compared to the turbine's characteristic timescale for dynamic inflow, the turbine's rotational inertia is expected to have a more dominant effect than the dynamic inflow effects for the current experimental study. It may be assumed that the rate of change of kinetic energy of the rotor is equal to the difference of the instantaneous wind power entering the rotor and the instantaneous power generated $P(t)$ leaving the rotor.[42] Then, the energy balance of the system can be expressed in the form of

$$\begin{aligned} \frac{dE_{rot}(t)}{dt} &= -P(t) + \frac{C_P \cos^2\psi \rho A u^3(t)}{2}, \\ E_{rot}(t) &= \frac{I\Omega(t)^2}{2}, \\ P(t) &= \tau(t)\Omega(t), \end{aligned} \tag{1}$$

where E_{rot} is the rotational kinetic energy, I is the rotor moment of inertia determined based on the three-dimensional (3D) CAD model from SolidWorks, Ω is the rotational velocity, τ is the electrical torque, and C_P is the time averaged power coefficient. With the inputs of incoming velocity properties such as wind flow fluctuation amplitude, frequency, and mean velocity, Eq. (1) allows to determine the time-series of unsteady power output $P(t)$ across various periodically oscillating winds and turbine yaw angles, and the numerical solutions of $P(t)$ based on this model are superimposed as red lines in Fig. 2. In general, both the magnitude and phase of the modeled $P(t)$ exhibited a consistent alignment with the experimental results. In particular, the prediction of $P(t)$ via Eq. (1) outperformed significantly when compared to "naive" estimation in the form of $P_{\text{naive}}(t) = C_P \cos^2\psi \rho A u^3(t)$, which exhibited significant overestimation and phase shifting with respect to the measured data as shown in Fig. 2. This highlighted the impacts of turbine rotor inertia on modulating its response to periodically oscillating winds and mitigating power output fluctuations. The intensity of unsteady turbine power output was then characterized by its standard deviations, σ_P, across all investigated cases, as summarized in Fig. 3. Overall, the magnitudes of non-dimensional power fluctuations σ_P/P_0 increased with the growth of flow fluctuation intensity U_A/U_0, whereas they exhibited a decreasing trend with the growth of yaw angle. The distribution of σ_P/P_0 was also compared with the predictions from Eq. (1) and the "naive" estimation, where distinctive overestimations of power

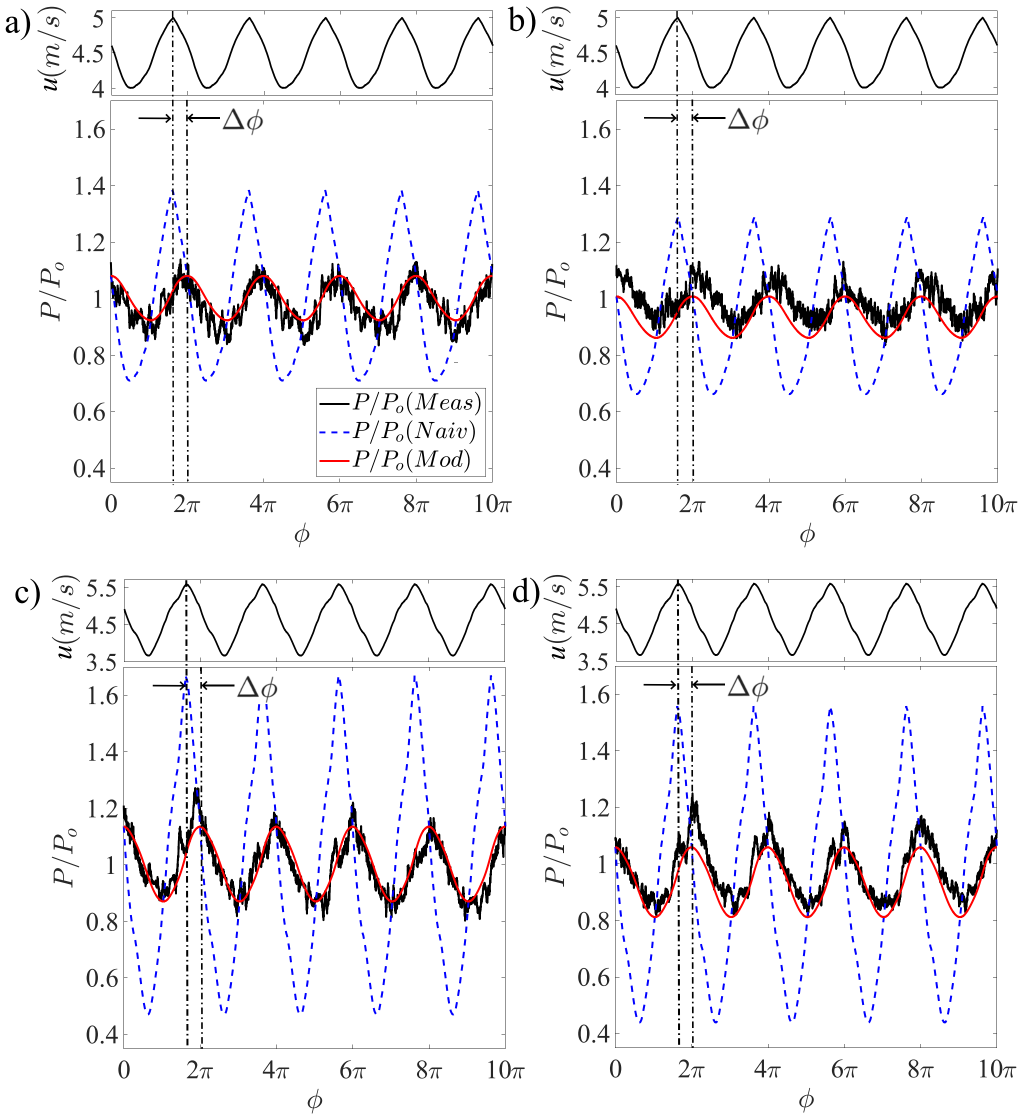

FIG. 2. The normalized measured, naive, and modeled unsteady power output, P/P_0 as a function of phase angle, ϕ, for selected cases. (a) $\psi = 0^\circ$, $U_A/U_0 = 0.11$, and $k = 0.27$; (b) $\psi = 15^\circ$, $U_A/U_0 = 0.11$, and $k = 0.27$; (c) $\psi = 0^\circ$, $U_A/U_0 = 0.18$, and $k = 0.27$; and (d) $\psi = 15^\circ$, $U_A/U_0 = 0.18$, and $k = 0.27$.

output fluctuations were observed based on the "naive" estimation. The matching between experimental data and this reduced-order model further validated its capability for analyzing unsteady turbine power outputs within periodically oscillating winds.

In order to gain a deeper comprehension of the phase shifting between $u(t)$ and $P(t)$ within periodically oscillating flows observed in Fig. 2, the reduced-order model from Eq. (1) can be reorganized in the following format as

$$\begin{aligned} u(t) &= U_0 + U_A \sin(2\pi f t), \\ \frac{dP}{dt} + \frac{1}{t_i}P &= \frac{1}{2t_i} C_P \cos^2\psi \rho A u^3(t), \end{aligned} \tag{2}$$

where $t_i = \frac{I\Omega}{2\tau}$ is the inertial timescale. The steady-state analytical solution of Eq. (2) can be expressed in the following format:

$$\begin{aligned} P(t) = C_1 + C_2 \frac{\sin(2\pi f t + \phi_1)}{(4\pi^2 f^2 t_i^2 + 1)^{1/2}} + C_3 \frac{\sin(4\pi f t + \phi_2)}{(16\pi^2 f^2 t_i^2 + 1)^{1/2}} \\ + C_4 \frac{\sin(6\pi f t + \phi_3)}{(36\pi^2 f^2 t_i^2 + 1)^{1/2}}, \end{aligned} \tag{3}$$

where the coefficients C_1–C_4 of each term and associated phase lags ϕ_1–ϕ_3 are

$$\begin{aligned} C_1 &= \frac{C_P \cos^2\psi \rho A U_0}{2}\left(U_0^2 + \frac{3U_A^2}{2}\right) \\ C_2 &= \frac{3C_P \cos^2\psi \rho A U_A}{2}\left(U_0^2 + \frac{U_A^2}{4}\right) \\ C_3 &= -\frac{C_P \cos^2\psi \rho A U_0 U_A^2}{4} \quad C_4 = -\frac{C_P \cos^2\psi \rho A U_A^3}{8} \end{aligned} \tag{4}$$

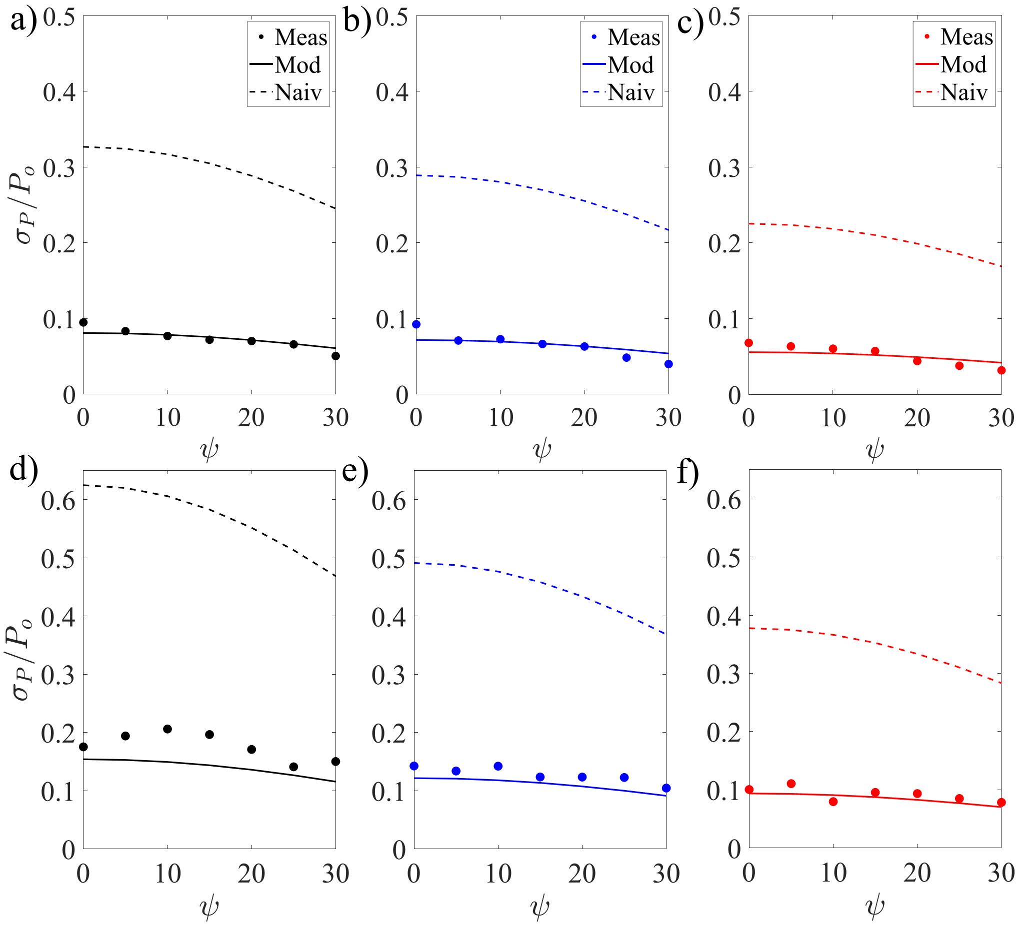

FIG. 3. Comparison of measured, naïve, and modeled normalized standard deviation of power output, σ_P/P_o, as a function of yaw angle, ψ across all investigated case. (a) $U_A/U_0 = 0.16$, and $k = 0.16$; (b) $U_A/U_0 = 0.14$, and $k = 0.21$; (c) $U_A/U_0 = 0.11$, and $k = 0.27$; (d) $U_A/U_0 = 0.24$, and $k = 0.16$; (e) $U_A/U_0 = 0.21$, and $k = 0.21$; (f) $U_A/U_0 = 0.18$, and $k = 0.27$.

and

$$\phi_1 = -\tan^{-1}(2\pi f t_i) \quad \phi_2 = \tan^{-1}\left(\frac{1}{4\pi f t_i}\right) \quad \phi_3 = -\tan^{-1}(6\pi f t_i). \tag{5}$$

Considering that U_A is much lower than U_0, the coefficients of high-order harmonic terms, i.e., C_3 and C_4, are much smaller than C_2. As a first-order approximation, the phase lag $\Delta\phi$ between $u(t)$ and $P(t)$ can be estimated as ϕ_1, i.e.,

$$\Delta\phi = -\phi_1 = \tan^{-1}(2\pi f t_i). \tag{6}$$

Figure 4 depicts the comparison of phase lag $\Delta\phi$ predicted by Eq. (6) and those obtained from numerically solving Eq. (1). $\Delta\phi$ from experimental measurements averaged across all yaw angles and flow fluctuation amplitudes under a given k are also included. Overall, the analytical solution with first-order approximation agrees well with numerical solutions and the measured phase lag. Results from this analytical model highlighted that for a turbine operating in periodically oscillating wind environments, the phase lag between power output

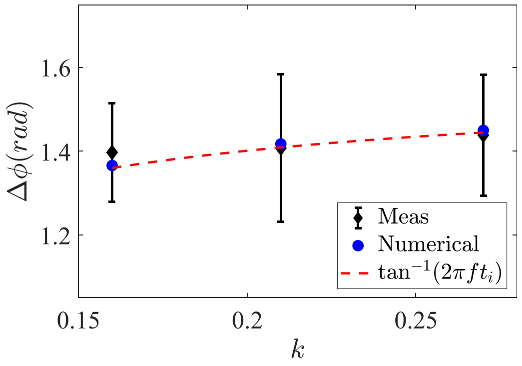

FIG. 4. Phase lag $\Delta\phi$ between power output $P(t)$ and incoming flow $u(t)$ as a function of non-dimensional flow fluctuation frequency k obtained from measured time series, numerical solutions of Eq. (1), and the first-order approximation by Eq. (6). The experimental data are averaged across all yaw angles and flow fluctuation amplitudes under a given k, where the error bar represents standard deviation across yaw angles and flow fluctuation amplitudes.

and incoming wind flow increases with the growth of turbine inertial timescale and wind fluctuation frequency, whereas the turbine yaw angle and flow fluctuation intensity have a minor influence on phase lag.

B. Unsteady aerodynamic loads on turbine tower

In a manner akin to the fluctuations of power outputs, the unsteady aerodynamic loads of the turbine under periodically oscillating winds were first characterized via the representative time series of the normalized thrust loads F_T/F_{T0} as depicted in Fig. 5. Similar to $P(t)$, $F_T(t)$ exhibited sinusoidal variations across time, and the mean thrust force decreased with the growth of the yaw angle. It is worth noting that, in contrast to power output fluctuations, which exhibited a consistent phase delay with the instantaneous incoming wind speed $u(t)$, the phase difference between $F_T(t)$ and $u(t)$ is negligible; this indicates that the fluctuations of aerodynamic loads on turbine towers in periodically oscillating winds are non-sensitive to the inertia effect of the rotor. Indeed, this phenomenon can be interpreted by inspecting the sensitivity of thrust coefficient C_T as a function of the instantaneous turbine tip speed ratio $\lambda(t) = \Omega(t)R/u(t)$, where R is the rotor radius. Figure 5 illustrates the representative time series of $\lambda(t)$ superimposed with $u(t)$. Overall, due to the rotor inertia effect and associated phase delay between $\Omega(t)$ and $u(t)$, $\lambda(t)$ changes with time from

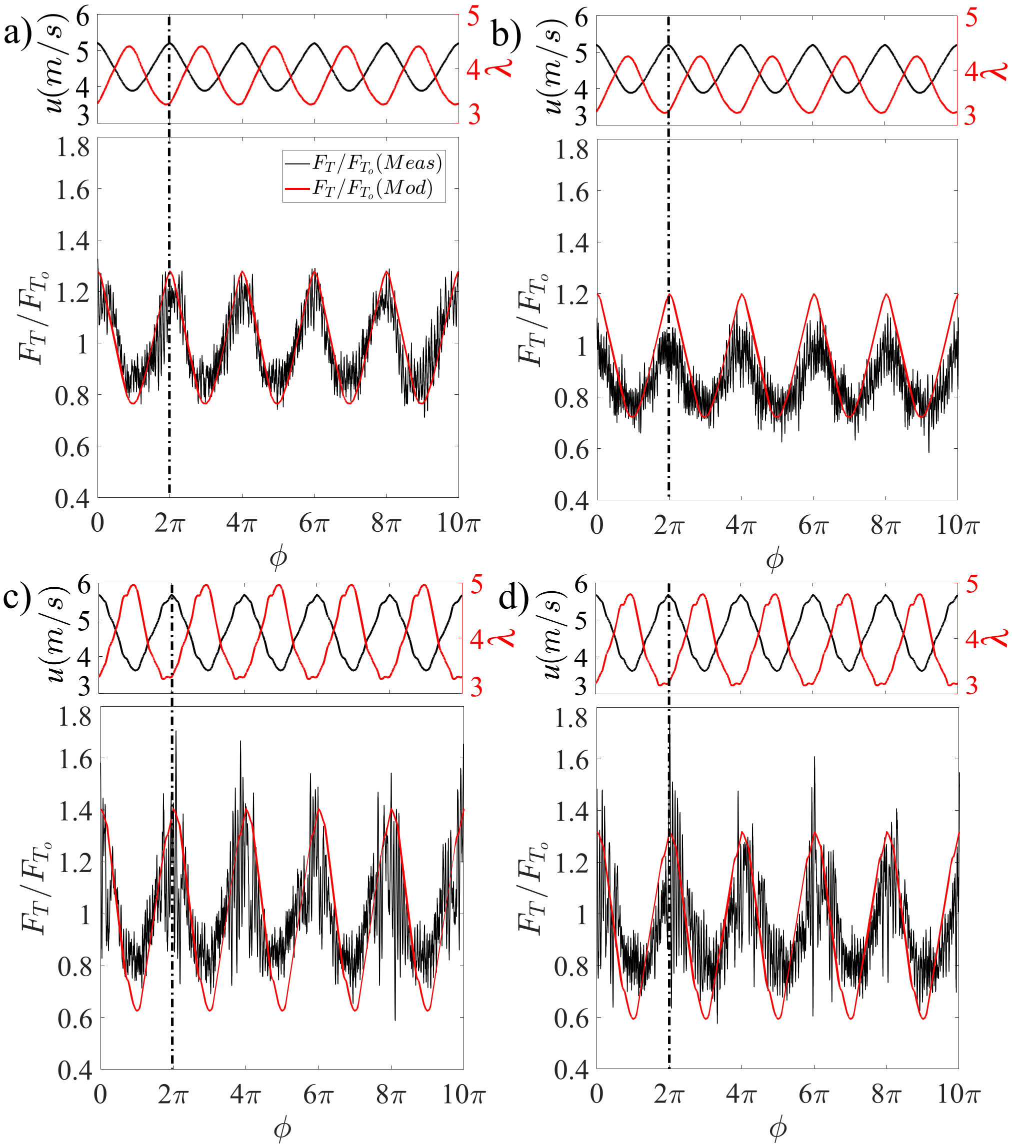

FIG. 5. The normalized measured and modeled unsteady thrust force, F_T/F_{T_0}, as a function of phase angle, ϕ, for selected cases. (a) $\psi = 0°$, $U_A/U_0 = 0.14$, and $k = 0.21$; (b) $\psi = 15°$, $U_A/U_0 = 0.14$, and $k = 0.21$; (c) $\psi = 0°$, $U_A/U_0 = 0.21$, and $k = 0.21$; and (d) $\psi = 15°$, $U_A/U_0 = 0.21$, and $k = 0.21$.

3.2 to 5. Within this range of $\lambda(t)$, the variation of turbine thrust coefficient is less than 4 % (i.e., $C_T = 0.77 \pm 0.3$) according to the rotor aerodynamic design.[33] Therefore, due to the low sensitivity of C_T to $\lambda(t)$, the bulk wind loads acting on the turbine are mostly governed by the instantaneous incoming flow speed, and the phase delay between $u(t)$ and $F_T(t)$ is negligible.

Owing to the minor fluctuations of C_T across the $\lambda(t)$, the unsteady aerodynamic loads of turbine within periodically oscillating winds can be estimated as a function of instantaneous $u(t)$ and turbine properties in the form of

$$F_T(t) = \frac{C_T \rho A u^2(t) \cos^{\alpha}(\psi)}{2}, \qquad (7)$$

where $\alpha = 1.5$ describes the decaying rate of time-averaged thrust coefficient $\bar{C}_T$ with respect to ψ, which was determined through empirical fitting of the measured data. By substituting the incoming periodically oscillating flow into Eq. (7), the unsteady thrust force can be estimated, shown as red lines in Fig. 5. Overall, the simple model allows it to reasonably capture the unsteady aerodynamic loads under various wind conditions and yaw misalignments. The good matching between experimental data and Eq. (7) is further reflected by the comparison of the standard deviation of thrust force as summarized in Fig. 6, where σ_{F_T} decreased with the growth of ψ due to the smaller projected rotor swept area and increased with the growth of flow fluctuation intensity owing to the stronger incoming wind velocity fluctuations.

C. Wake flow statistics

This section aims to assess the impact of yaw misalignment on various turbulence statistics, including mean velocity, flow unsteadiness, compensated velocity spectra, and wake signal transportation downstream of a turbine subjected to periodically oscillating incoming flow. These results are expected to provide insights for analyzing the performance of downstream turbines in periodically oscillating wind environments. First, Fig. 7 shows the mean normalized stream-wise wake velocity, U/U_0, at hub height with $\psi = 0^\circ, 15^\circ$, and 30° at nondimensional flow fluctuation frequency of $k = 0.27$ and flow

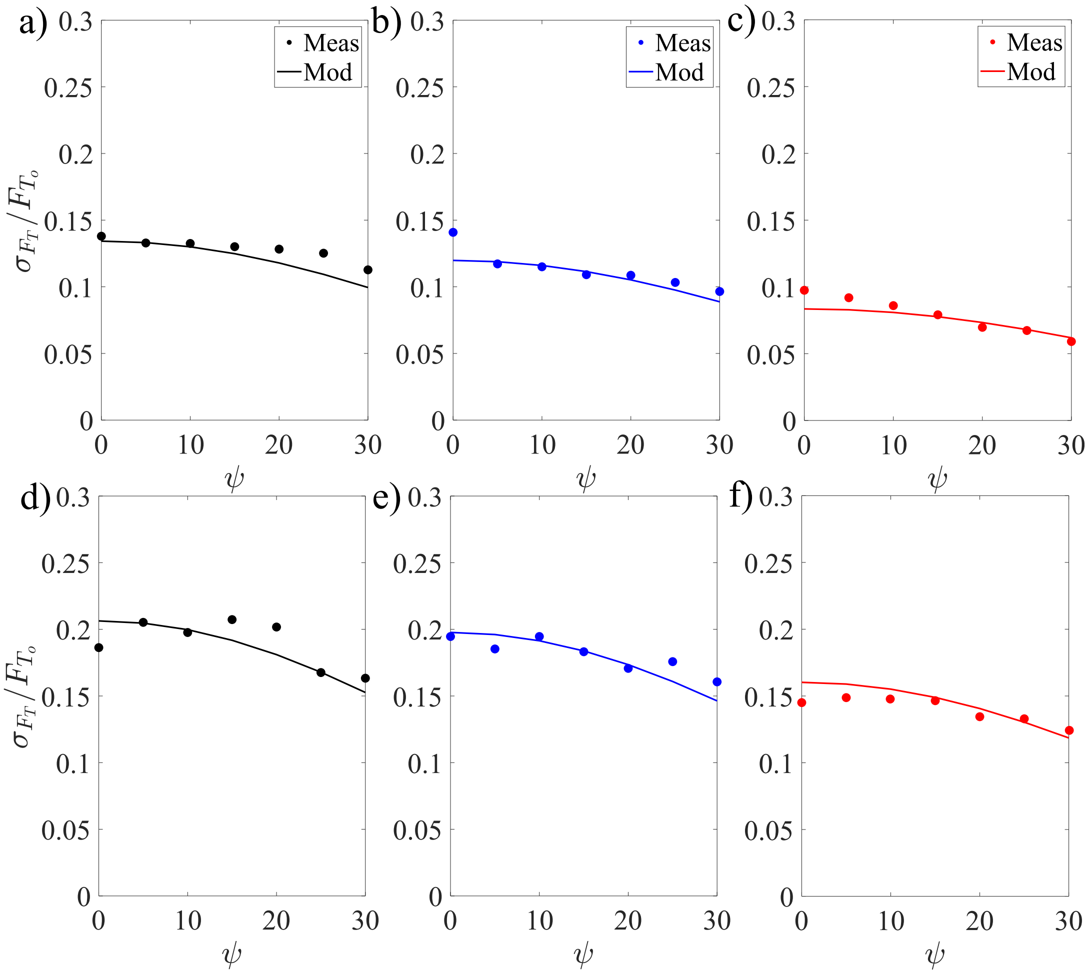

FIG. 6. Comparison of measured and modeled normalized standard deviation of thrust-force, σ_{F_T}/F_{T0}, as a function of yaw angle, ψ. (a) $U_A/U_0 = 0.16$ and $k = 0.16$; (b) $U_A/U_0 = 0.14$ and $k = 0.21$; (c) $U_A/U_0 = 0.11$ and $k = 0.27$; (d) $U_A/U_0 = 0.24$ and $k = 0.16$; (e) $U_A/U_0 = 0.21$ and $k = 0.21$; and (f) $U_A/U_0 = 0.18$ and $k = 0.27$.

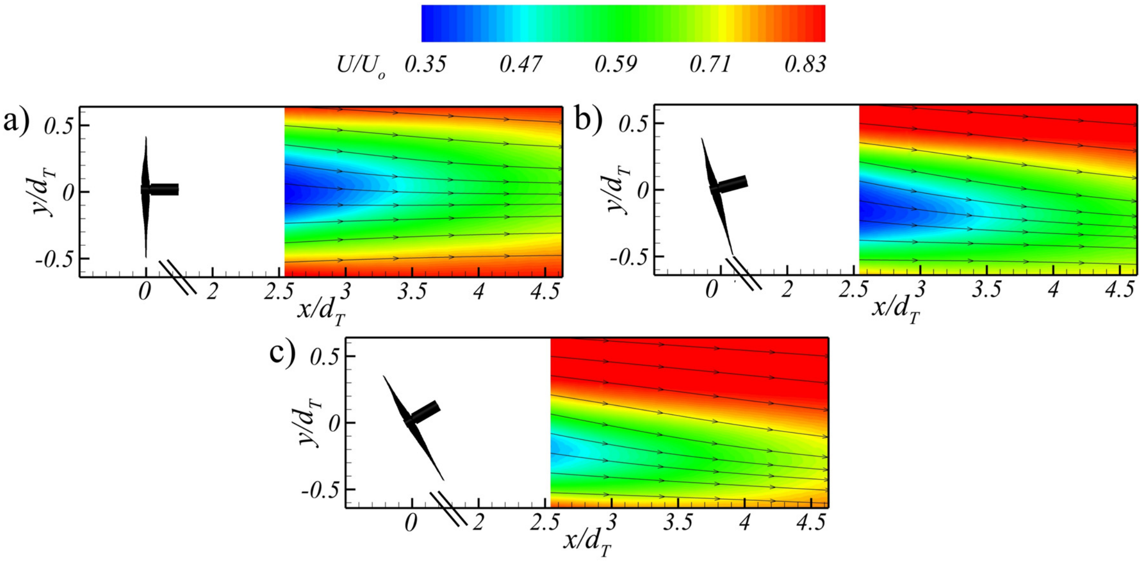

FIG. 7. Normalized mean stream-wise velocity distribution, U/U_0, in the wake of turbine at a non-dimensional flow fluctuation frequency of $k = 0.27$ and flow fluctuation intensity of U_A/U_0=0.18 under different yaw misalignment angles $\psi =$ (a) 0°, (b) 15°, and (c) 30°. The superimposed streamlines highlight the induced span-wise velocities at high yaw angles.

fluctuation intensity of $U_A/U_0 = 0.18$. Overall, similar to previous studies of turbines in the absence of periodically oscillating winds,[22,43,44] the yaw misalignment modulated the mean velocity profile of turbine wake flow via two aspects. First, the growth of the yaw angle led to a monotonous increase in wake flow deflection from the centerline ($y = 0$). This phenomenon can be observed more clearly by examining the superimposed streamlines, which revealed a significant span-wise flow with ($V < 0$) when ψ increased to 30° [Fig. 7(c)]. In such a scenario, the wake impinging on a downstream turbine will no longer be perpendicular to their rotor surfaces, which is expected to enhance their aerodynamic loads perpendicular to the incoming wind direction. On the other hand, yaw misalignment reduces the wake velocity deficit and narrows the wake width, indicating a stronger effect of wake mixing and flow recovery. This phenomenon is clearly reflected in Fig. 8 with selected transverse profiles of normalized stream-wise velocity deficit, $\Delta U/U_0$, at various downstream locations, $x/d_T = 2.6, 3.6$, and 4.6. In particular, the span-wise averaged velocity deficit was reduced by approximately 36% at $\psi = 30°$ in the near-wake region when compared to the base case, which highlighted the effectiveness of wake steering in enhancing the mean power output of downstream turbines.

The impact of turbine yaw misalignment in modulating the unsteady wake flow dynamics within periodically oscillating wind

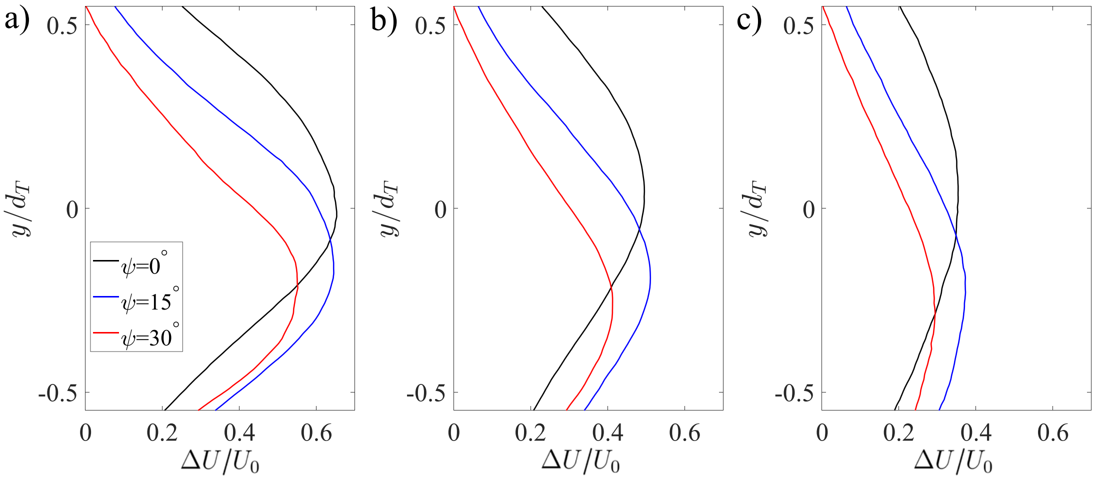

FIG. 8. Transverse profiles of mean stream-wise velocity deficit, $(U_0 - U)/U_0$, in the wake of the turbine at a non-dimensional flow fluctuation frequency of $k = 0.27$ and flow fluctuation intensity of U_A/U_0=0.18 across different yaw misalignment angles ψ at (a) x/d_T=2.6, (b) x/d_T=3.6, and (c) x/d_T=4.6.

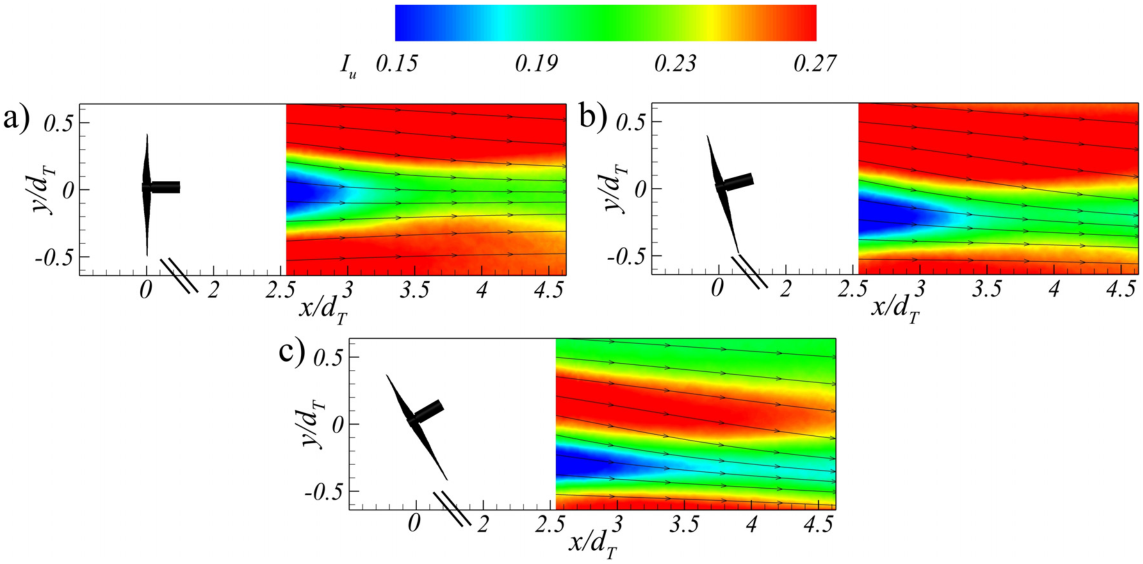

FIG. 9. Distribution of flow unsteadiness, $I_u = \sigma_u/U_0$, in the wake of turbine at a non-dimensional flow fluctuation frequency of $k = 0.27$ and flow fluctuation intensity of U_A/U_0=0.18 under different yaw misalignment angles ψ = (a) 0°, (b) 15°, and (c) 30°.

environments was first illustrated by the examination of flow unsteadiness distribution, denoted as $I_u = \sigma_u/U_0$, as depicted in Figs. 9 and 10. At $\psi = 0^\circ$, the wake flow unsteadiness exhibits local peaks at $y/d_T \pm 0.5$ as a result of the significant velocity shear immediately downstream of the turbine tips shown in Fig. 7, and reaches a minimum at $y/d_T = 0$. The increase in ψ caused a gradual shift of the peak of I_u toward the rotor center, where the maximum I_u was observed close to $y = 0$ when ψ reached 30°. To highlight the role of the turbine rotor in modulating flow fluctuation intensities within periodically oscillating winds, the difference in flow unsteadiness between incoming and wake flows, $\Delta I_u = (\sigma_u - \sigma_{u0})/U_0$, is shown in Fig. 11. Indeed, outside the wake centerline region, where the local wind flow dynamics are highly modulated by the rotor hub, the overall wake flow fluctuation intensity was enhanced compared to that from the incoming periodically oscillating wind, especially in the vicinity of wake flow edges; this indicated that for wind farms within periodically oscillating flow environments, the downstream turbines may exhibit even stronger power and aerodynamic load fluctuations compared to their upstream counterparts. To gain a deeper comprehension of such unsteady wake flow dynamics, the pre-multiplied spectral difference of stream-wise velocity, $\Delta(Ef) = Ef - E_{in}f$, between the wake and incoming flows at a normalized downstream distance of $x/d_T = 4.6$ is depicted in Fig. 12 at various span-wise distances and yaw angles under $k = 0.27$ and $U_A/U_0 = 0.18$. In this context, f represents the

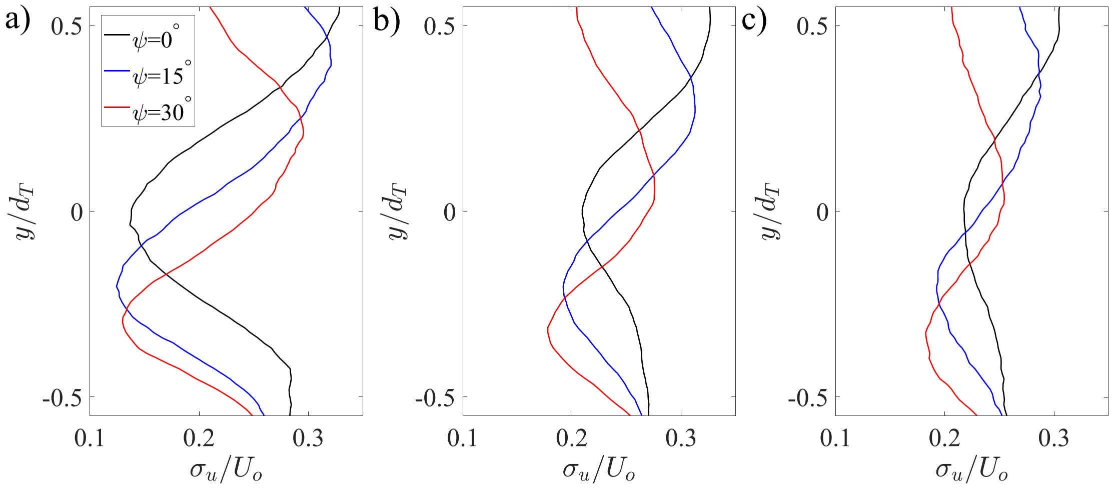

FIG. 10. Transverse profiles of flow unsteadiness, $I_u = \sigma_u/U_0$, in the wake of the turbine at a non-dimensional flow fluctuation frequency of $k = 0.27$ and flow fluctuation intensity of U_A/U_0=0.18 across different yaw misalignment angles ψ at (a) x/d_T=2.6, (b) x/d_T=3.6, and (c) x/d_T=4.6.

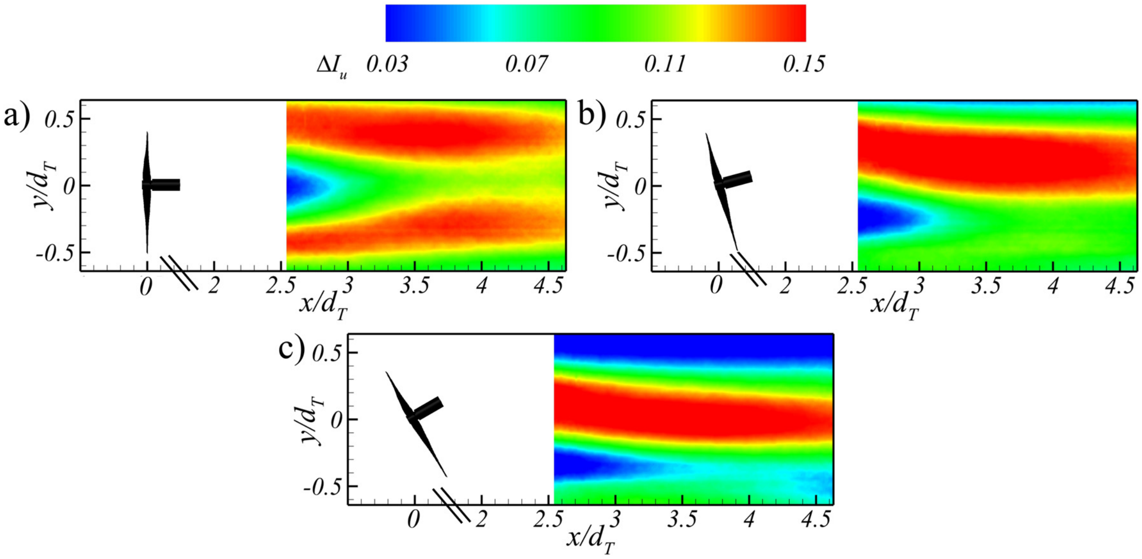

FIG. 11. Relative flow unsteadiness distribution, $\Delta I_u = (\sigma_u - \sigma_{u0})/U_0$, in the wake of turbine at a non-dimensional flow fluctuation frequency of $k = 0.27$ and flow fluctuation intensity of U_A/U_0=0.18 under different yaw misalignment angles ψ = (a) 0°, (b) 15°, and (c) 30°.

frequency related to turbulence scales, while E represents the spectral energy density at each frequency. The compensated velocity spectra $[\Delta(Ef)]$ will assist us in understanding the turbulence scales in the wake of the turbine under periodically oscillating inflows and yaw misalignment in comparison to incoming wind flows. In general, regardless of turbine yaw angle, the wake flow energy was enhanced at high frequency ranges of $fd_T/U_0 > 0.1$, which corresponds to the small-scale turbulent vortices produced by the turbine rotor. With the growth of turbine yaw angle, the overall intensity of $\Delta(Ef)$ reduced, and the high-frequency fluctuations in the wake flow shifted toward the $y < 0$ regions due to the deflection of wake as discussed in Fig. 8. Our experimental measurements revealed that yaw misalignment of the turbine not only decreases the velocity deficits in the wake region but also mitigates wind velocity fluctuations across a broad range of frequency components under periodically oscillating wind conditions. Specifically, at potential downstream turbine locations, $x/d_T = 4.6$, yaw misalignment from 0° to 30° reduced the span-wise averaged velocity deficits by 36% and span-wise averaged wind velocity fluctuations by 14%. This suggests that yaw misalignment could enhance the performance and stability of wind farms by improving conditions for downstream turbines in periodically oscillating wind environments.

Finally, the correlation strength of wake flow fluctuations along stream-wise direction across various span-wise positions and turbine yaw angles was investigated; this helps to reflect the correlation of unsteady power outputs between upstream and downstream turbines and provide insights to determine the power output fluctuations over the entire wind farm under periodically oscillating flows. In this work, the correlation strength is quantified by the cross-correlations on the time series of stream-wise velocities at two locations within the wake flow region:

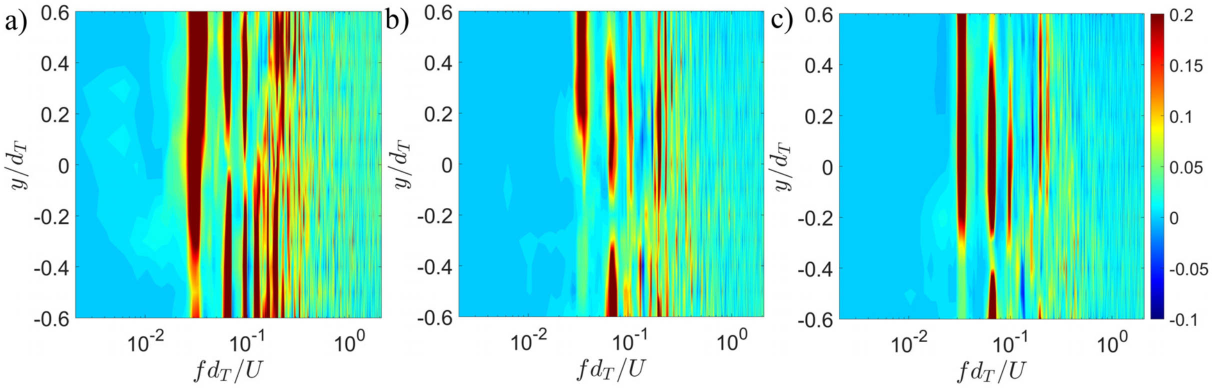

FIG. 12. Compensated velocity spectra along the span-wise direction, $\Delta(Ef)$, at a non-dimensional flow fluctuation frequency of $k = 0.27$ and flow fluctuation intensity of U_A/U_0=0.18 under different yaw misalignment angles ψ = (a) 0°, (b) 15°, and (c) 30°.

$$\eta(\tau)|_{x=2.6d_T,x=2.6d_T+\delta x} = \frac{\langle u_{x=2.6d_T}(t)u_{x=2.6d_T+\delta x}(t+\tau)\rangle}{\sigma_{u,x=2.6d_T}\sigma_{u,x=2.6d_T+\delta x}}. \tag{8}$$

Equation (8) describes the cross correlation coefficient of stream-wise flow velocity fluctuations at $x = 2.6d_T$ and downstream locations $2.6d_T + \delta x$. Representative variation of $\eta(\tau)$ under $\psi = 0°$ along $y = 0$ is shown in Fig. 13(a). Regardless of the gap distance δx, with a specific time delay (Δt), η reaches the local maximum η_{max} (marked by the red dashed lines), indicating that the footprint of upwind flow fluctuations is transported to the downstream location. Overall, with the growth of gap distance, η_{max} exhibited monotonous decay; this is expected to result in the decoupling of up- and downstream turbine power output fluctuations within periodically oscillating winds. To further investigate the evolution of wake velocity correlation strength, the distribution of η_{max} as a function of δx, turbine yaw angle ψ, and span-wise locations is summarized in Figs. 13(b)–13(d). The results highlighted that on the trailing edge side of the wake flow region, i.e., $y/d_T = -0.5$ [Fig. 13(b)], the growth of turbine yaw angle led to a gradual decrease in η_{max}. Note that yaw misalignment deflected the turbine wake flow toward the rotor trailing edge, and these wake flows, which contain small-scale turbulent vortices as shown in Fig. 12, are expected to disturb the wind velocity correlations from the background periodically oscillating flow. On the other hand, at $y = 0$ [i.e., wake centerline for the base case, Fig. 13(c)], η_{max} exhibited distinct growth with ψ due to the mitigation of wake flow impacts in this region induced by yaw misalignment. Finally, minor variations of η_{max} were observed downstream of the rotor leading edge at $y/d_T = 0.5$ [Fig. 13(d)], indicating that background periodically oscillating wind flow dominates the wake velocity transport in this region regardless of ψ.

IV. CONCLUSION

In this study, wind tunnel experiments were performed to examine the unsteady power production and aerodynamic loads of a turbine under successive incoming periodically oscillating flows and various

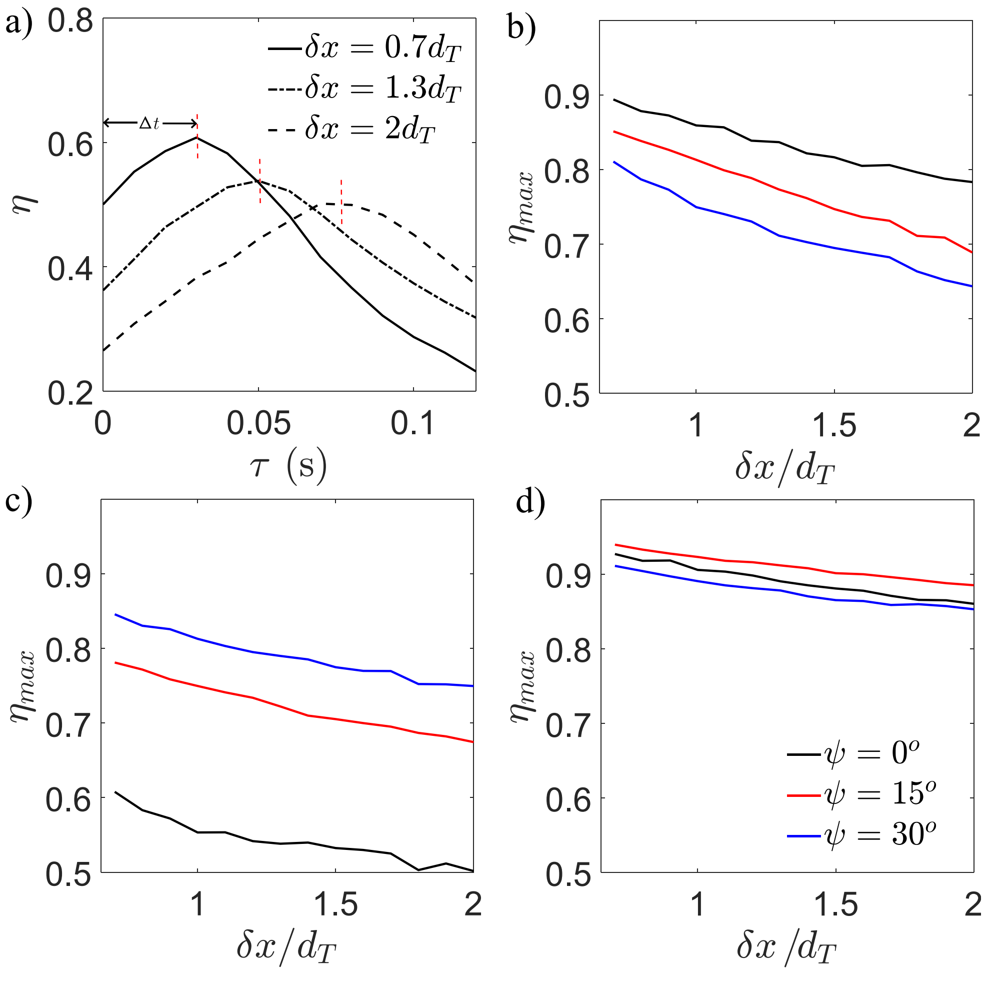

FIG. 13. (a) Distribution of cross correlation function $\eta(\tau)$ for selected cases under $\psi = 0°$ at $y/d_T = 0$ at a non-dimensional flow fluctuation frequency of $k = 0.27$ and flow fluctuation intensity of U_A/U_o=0.18. (b)–(d) The evolution of maximum correlation coefficient η_{max} along stream-wise direction at various span-wise locations and yaw misalignment angles: (b) $y/d_T = -0.5$ (trailing edge), (c) $y/d_T = 0$ (center), and (d) $y/d_T = 0.5$ (leading edge).

yaw misalignment angles. Overall, stronger turbine power output fluctuation occurs under smaller yaw misalignment angles and larger flow fluctuation intensities. The experimental results highlighted the distinctive phase lag between wind velocity fluctuations and unsteady power output due to the inertia of the turbine rotor. Based on the coupling between time-varying wind speeds, rotational kinetic energy, and turbine power output, reduced-order models were established to elucidate the evolution of power fluctuation intensity and phase lag. The results revealed that higher phase lag occurs with the growth of turbine inertial timescale and wind fluctuation frequency. In general, the evolution of unsteady aerodynamic loads on turbine towers exhibited a similar trend to that of power fluctuations. However, the phase lag between the aerodynamic load and incoming winds was negligible owing to the low sensitivity of the thrust load coefficient as a function of the time-varying turbine tip speed ratio within periodically oscillating winds.

The examination of wake characteristics has demonstrated that when the turbine yaw misalignment angle increases, the flows can be notably redirected, leading to enhanced wake velocities and reduced flow unsteadiness. The operation of turbines in periodically oscillating wind environments can amplify the wake velocity fluctuation intensity when compared to incoming flow, which brings potential challenges regarding the enhancement of the unsteady aerodynamic loads on downstream turbines. Overall, the growth of the turbine yaw misalignment angle significantly enhances the wake velocity correlations along the stream-wise direction downstream of the turbine hub location, whereas such correlations remain nearly constant downstream of the turbine leading edge. Subsequent research endeavors to address the challenges posed by the impact of dynamic inflow effects in the presence of periodically oscillating inflow through experimental investigations and OpenFAST simulations.

ACKNOWLEDGMENTS

This paper is based upon work partially supported by the National Science Foundation under Award Nos. 1916715 and 1916776 (I/UCRC for Wind Energy, Science, Technology, and Research) and from the industry members of WindSTAR I/UCRC. Any opinions, findings, and conclusions or recommendations expressed in this material are those of the author(s) and do not necessarily reflect the views of the National Science Foundation or the sponsors.

AUTHOR DECLARATIONS

Conflict of Interest

The authors have no conflicts to disclose.

Author Contributions

Emmanuvel Joseph Aju: Conceptualization (equal); Investigation (lead); Methodology (lead); Writing – original draft (lead). **Pengyao Gong:** Investigation (supporting); Methodology (supporting). **Devesh Kumar:** Methodology (supporting). **Mario A. Rotea:** Conceptualization (equal); Supervision (equal); Writing – review & editing (equal). **Yaqing Jin:** Conceptualization (lead); Supervision (lead); Writing – review & editing (lead).

DATA AVAILABILITY

The data that support the findings of this study are available from the corresponding author upon reasonable request.

APPENDIX: ANALYTICAL SOLUTION OF ENERGY BALANCE EQUATION

This section presents the process of obtaining the analytical solution to Eq. (2) by starting from the energy balance equation [Eq. (1)], as shown below:

$$\begin{aligned} \frac{dE_{rot}(t)}{dt} &= -P(t) + \frac{C_P \cos^2\psi \rho A u^3(t)}{2}, \\ E_{rot}(t) &= \frac{I\Omega(t)^2}{2}, \\ P(t) &= \tau(t)\Omega(t). \end{aligned} \tag{A1}$$

The inertial timescale is defined as

$$t_i = \frac{I\Omega}{2\tau}. \tag{A2}$$

By substituting Eq. (A2) in Eq. (A1), we can reorganize the governing differential equation in the following format:

$$\frac{dP}{dt} + \frac{1}{t_i}P = \frac{1}{2t_i} C_P \cos^2\psi \rho A u^3(t). \tag{A3}$$

The sinusoidal incoming flow is given as follows:

$$u(t) = U_0 + U_A \sin(2\pi f t). \tag{A4}$$

By substituting the sinusoidal incoming flow in Eq. (A3), we can obtain a linear non-homogeneous differential equation, which can be solved using integrating factor, $I = e^{t/t_i}$,. The steps are provided below,

$$\frac{dP}{dt} + \frac{1}{t_i}P = \frac{1}{2t_i} C_P \cos^2\psi \rho A (U_0 + U_A \sin(2\pi f t))^3. \tag{A5}$$

Multiplying both sides of Eq. (A5) by integrating factor, we obtain

$$e^{t/t_i}\frac{dP}{dt} + \frac{e^{t/t_i}}{t_i}P = \frac{e^{t/t_i}}{2t_i} C_P \cos^2\psi \rho A (U_0 + U_A \sin(2\pi f t))^3. \tag{A6}$$

The left hand side of the equation can be simplified to obtain

$$\frac{d(Pe^{t/t_i})}{dt} = \frac{e^{t/t_i}}{2t_i} C_P \cos^2\psi \rho A (U_0 + U_A \sin(2\pi f t))^3. \tag{A7}$$

By expanding the right hand side and integrating both sides, we obtain

$$\begin{aligned} P(t)e^{t/t_i} = C_1 e^{t/t_i} &+ C_2 e^{t/t_i} \frac{\sin(2\pi f t + \phi_1)}{(4\pi^2 f^2 t_i^2 + 1)^{1/2}} \\ &+ C_3 e^{t/t_i} \frac{\sin(4\pi f t + \phi_2)}{(16\pi^2 f^2 t_i^2 + 1)^{1/2}} \\ &+ C_4 e^{t/t_i} \frac{\sin(6\pi f t + \phi_3)}{(36\pi^2 f^2 t_i^2 + 1)^{1/2}} + C_5. \end{aligned} \tag{A8}$$

By dividing both sides by e^{t/t_i}, we obtain

$$P(t) = C_1 + C_2 \frac{\sin(2\pi f t + \phi_1)}{(4\pi^2 f^2 t_i^2 + 1)^{1/2}} + C_3 \frac{\sin(4\pi f t + \phi_2)}{(16\pi^2 f^2 t_i^2 + 1)^{1/2}} + C_4 \frac{\sin(6\pi f t + \phi_3)}{(36\pi^2 f^2 t_i^2 + 1)^{1/2}} + C_5 e^{-t/t_i}. \tag{A9}$$

As time, t, increases and reaches steady state, the fifth term in the solution vanishes resolving into the steady state analytical solution as

$$P(t) = C_1 + C_2 \frac{\sin(2\pi f t + \phi_1)}{(4\pi^2 f^2 t_i^2 + 1)^{1/2}} + C_3 \frac{\sin(4\pi f t + \phi_2)}{(16\pi^2 f^2 t_i^2 + 1)^{1/2}} + C_4 \frac{\sin(6\pi f t + \phi_3)}{(36\pi^2 f^2 t_i^2 + 1)^{1/2}}, \tag{A10}$$

where the coefficients are given as

$$\begin{gathered} C_1 = \frac{C_P \cos^2\psi \rho A U_0}{2}\left(U_0^2 + \frac{3U_A^2}{2}\right), \\ C_2 = \frac{3C_P \cos^2\psi \rho A U_A}{2}\left(U_0^2 + \frac{U_A^2}{4}\right), \\ C_3 = -\frac{C_P \cos^2\psi \rho A U_0 U_A^2}{4}, \quad C_4 = -\frac{C_P \cos^2\psi \rho A U_A^3}{8}. \end{gathered} \tag{A11}$$

The analytical solution yields the power variations of the turbines as the output, while the parameters of the incoming velocity time series, such as mean, amplitude, and frequency, serve as inputs to the analytical solution.

REFERENCES

[1] EIA, *Electricity in the United States—Energy Explained, Your Guide to Understanding Energy* (EIA, 2019). https://www.eia.gov/energyexplained/index.cfm?page=electricity_in_the_united_states.

[2] P. C. Johnston, *Climate Risk and Adaptation in the Electric Power Sector* (Asian Development Bank, 2012).

[3] S. C. Pryor and R. J. Barthelmie, "Climate change impacts on wind energy: A review," Renewable Sustain. Energy Rev. **14**(1), 430–437 (2010).

[4] D. Carvalho, A. Rocha, M. Gómez-Gesteira, and C. Silva Santos, "Potential impacts of climate change on European wind energy resource under the CMIP5 future climate projections," Renewable Energy **101**, 29–40 (2017).

[5] P. S. Veers, T. D. Ashwill, H. J. Sutherland, D. L. Laird, D. W. Lobitz, D. A. Griffin, J. F. Mandell, W. D. Musial, K. Jackson, M. Zuteck *et al.*, "Trends in the design, manufacture and evaluation of wind turbine blades," Wind Energy **6**(3), 245–259 (2003).

[6] A. C. Spassiani and M. S. Mason, "Application of self-organizing maps to classify the meteorological origin of wind gusts in Australia," J. Wind Eng. Ind. Aerodyn. **210**, 104529 (2021).

[7] S. Cao, Y. Tamura, N. Kikuchi, M. Saito, I. Nakayama, and Y. Matsuzaki, "A case study of gust factor of a strong typhoon," J. Wind Eng. Ind. Aerodyn. **138**, 52–60 (2015).

[8] G. Fang, L. Zhao, S. Cao, Y. Ge, and K. Li, "Gust characteristics of near-ground typhoon winds," J. Wind Eng. Ind. Aerodyn. **188**, 323–337 (2019).

[9] M. Pichault, C. Vincent, G. Skidmore, and J. Monty, "Lidar-based detection of wind gusts: An experimental study of gust propagation speed and impact on wind power ramps," J. Wind Eng. Ind. Aerodyn. **220**, 104864 (2022).

[10] E. Branlard, "Wind energy: On the statistics of gusts and their propagation through a wind farm," ECN Wind Memo **7**, 5–9 (2009).

[11] IEC ISO, "ISO/IEC 25010:2011" (2011).

[12] S. Fu, Y. Jin, Y. Zheng, and L. P. Chamorro, "Wake and power fluctuations of a model wind turbine subjected to pitch and roll oscillations," Appl. Energy **253**, 113605 (2019).

[13] S. Cioni, F. Papi, L. Pagamonci, A. Bianchini, N. Ramos-García, G. Pirrung, R. Corniglion, A. Lovera, J. Galván, and R. Boisard, "On the characteristics of the wake of a wind turbine undergoing large motions caused by a floating structure: An insight based on experiments and multi-fidelity simulations from the OC6 phase III project," Wind Energy Sci. Discuss. **2023**, 1–37.

[14] C. W. Schulz, S. Netzband, U. Özinan, P. W. Cheng, and M. Abdel-Maksoud, "Wind turbine rotors in surge motion: New insights into unsteady aerodynamics of floating offshore wind turbines (FOWTs) from experiments and simulations," Wind Energy Sci. **9**(3), 665–695 (2024).

[15] N. J. Wei and J. O. Dabiri, "Power-generation enhancements and upstream flow properties of turbines in unsteady inflow conditions," J. Fluid Mech. **966**, A30 (2023).

[16] N. J. Wei and J. O. Dabiri, "Phase-averaged dynamics of a periodically surging wind turbine," J. Renewable Sustain. Energy **14**(1), 013305 (2022).

[17] K. Zhou, N. Cherukuru, X. Sun, and R. Calhoun, "Wind gust detection and impact prediction for wind turbines," Remote Sens. **10**(4), 514 (2018).

[18] D. K. Kwon, A. Kareem, and K. Butler, "Gust-front loading effects on wind turbine tower systems," J. Wind Eng. Ind. Aerodyn. **104**, 109–115 (2012).

[19] V. Pakrashi, K. O'Sullivan, R. O'Shea, and J. Murphy, "Experimental responses of a monopile foundation with a wave energy converter attached," in *Proceedings of the Hydro 2013 International*, Chennai, India (Indian Institute of Technology Madras, 2013).

[20] I. Grant, P. Parkin, and X. Wang, "Optical vortex tracking studies of a horizontal axis wind turbine in yaw using laser-sheet, flow visualisation," Exp. Fluids **23**(6), 513–519 (1997).

[21] I. Grant and P. Parkin, "A DPIV study of the trailing vortex elements from the blades of a horizontal axis wind turbine in yaw," Exp. Fluids **28**(4), 368–376 (2000).

[22] M. Bastankhah and F. Porté-Agel, "Experimental and theoretical study of wind turbine wakes in yawed conditions," J. Fluid Mech. **806**, 506–541 (2016).

[23] M. F. Howland, J. Bossuyt, L. A. Martínez-Tossas, J. Meyers, and C. Meneveau, "Wake structure in actuator disk models of wind turbines in yaw under uniform inflow conditions," J. Renewable Sustain. Energy **8**(4), 043301 (2016).

[24] M. Churchfield, Q. Wang, A. Scholbrock, T. Herges, T. Mikkelsen, and M. Sjöholm, "Using high-fidelity computational fluid dynamics to help design a wind turbine wake measurement experiment," J. Phys.: Conf. Ser. **753**, 032009 (2016).

[25] J. Wang, S. Foley, E. M. Nanos, T. Yu, F. Campagnolo, C. L. Bottasso, A. Zanotti, and A. Croce, "Numerical and experimental study of wake redirection techniques in a boundary layer wind tunnel," J. Phys.: Conf. Ser. **854**, 012048 (2017).

[26] C. R. Shapiro, D. F. Gayme, and C. Meneveau, "Modelling yawed wind turbine wakes: A lifting line approach," J. Fluid Mech. **841**, R1 (2018).

[27] J. Schottler, J. Bartl, F. Mühle, L. Saetran, J. Peinke, and M. Hölling, "Wind tunnel experiments on wind turbine wakes in yaw: Redefining the wake width," Wind Energy Sci. **3**(1), 257–273 (2018).

[28] M. Bastankhah and F. Porté-Agel, "Wind tunnel study of the wind turbine interaction with a boundary-layer flow: Upwind region, turbine performance, and wake region," Phys. Fluids **29**(6), 065105 (2017).

[29] M. Bastankhah and F. Porté-Agel, "A wind-tunnel investigation of wind-turbine wakes in yawed conditions," J. Phys.: Conf. Ser. **625**, 012014 (2015).

[30] A. Ozbay, W. Tian, Z. Yang, and H. Hu, "Interference of wind turbines with different yaw angles of the upstream wind turbine," in *42nd AIAA Fluid Dynamics Conference and Exhibit* (AIAA, 2012), p. 2719.

[31] J. Bartl, F. Mühle, J. Schottler, L. Saetran, J. Peinke, M. Adaramola, and M. Hölling, "Wind tunnel experiments on wind turbine wakes in yaw: Effects of inflow turbulence and shear," Wind Energy Sci. **3**(1), 329–343 (2018).

[32] E. J. Aju, D. Bhamitipadi Suresh, and Y. Jin, "The influence of winglet pitching on the performance of a model wind turbine: Aerodynamic loads, rotating speed, and wake statistics," Energies **13**(19), 5199 (2020).

[33] M. Bastankhah and F. Porté-Agel, "A new miniature wind turbine for wind tunnel experiments. Part I: Design and performance," Energies **10**(7), 908 (2017).

[34] H. Liu, Y. Jin, N. Tobin, and L. P. Chamorro, "Towards uncovering the structure of power fluctuations of wind farms," Phys. Rev. E **96**(6), 063117 (2017).

[35] D. Kumar, M. A. Rotea, E. Joseph Aju, and Y. Jin, "Wind plant power maximization via extremum seeking yaw control: A wind tunnel experiment," Wind Energy **26**(3), 283–309 (2023).

[36] P. A. Brugger, C. D. Markfort, and F. Porté-Agel, "Field measurements of wake meandering at a utility-scale wind turbine with nacelle-mounted Doppler lidars," Wind Energy Sci. Discuss. **2021**, 1–22.

[37] M. Lin and F. Porté-Agel, "Wake meandering of wind turbines under dynamic yaw control and impacts on power and fatigue," Renewable Energy **223**, 120003 (2024).

[38] A. S. Wise and E. E. Bachynski, "Wake meandering effects on floating wind turbines," Wind Energy **23**(5), 1266–1285 (2020).

[39] H. Canet, P. Bortolotti, and C. L. Bottasso, "On the scaling of wind turbine rotors," Wind Energy Sci. **6**(3), 601–626 (2021).

[40] E. Mohammadi, R. Fadaeinedjad, and G. Moschopoulos, "Implementation of internal model based control and individual pitch control to reduce fatigue loads and tower vibrations in wind turbines," J. Sound Vib. **421**, 132–152 (2018).

[41] S. Mancini, K. Boorsma, G. Schepers, and F. Savenije, "A comparison of dynamic inflow models for the blade element momentum method," Wind Energy Sci. Discuss. **2022**, 1–27.

[42] N. Tobin, H. Zhu, and L. P. Chamorro, "Spectral behaviour of the turbulence-driven power fluctuations of wind turbines," J. Turbul. **16**(9), 832–846 (2015).

[43] H. Zong and F. Porté-Agel, "Experimental investigation and analytical modelling of active yaw control for wind farm power optimization," Renewable Energy **170**, 1228–1244 (2021).

[44] E. J. Aju, D. Kumar, M. Leffingwell, M. A. Rotea, and Y. Jin, "The influence of yaw misalignment on turbine power output fluctuations and unsteady aerodynamic loads within wind farms," Renewable Energy **215**, 118894 (2023).